PRAMANA
— journal of
physics

Vol. 42, No. 1,
January 1994
pp. 65–77

Ray tracing studies of a complete plane grating monochromator beam line

V S EDLABADKAR* and ASHOK PIMPALE
Inter University Consortium for DAE Facilities, University Campus, Indore 452001, India
*G. N. College of Science, Ballarpur 442701, India

MS received 24 July 1993; revised 11 October 1993

Abstract. Optical design of a plane grating monochromator beam line for X-ray spectroscopic studies to be installed on INDUS-1 is studied using ray tracing technique. The main components of the beam line are pre- and post-elliptical mirrors and the plane mirror-grating dispersing system. The ideal positions of the optical components are decided by using our analytical formulation of the Riemer's kinetic principle for reflecting synchrotron radiation onto the same spot of the dispersing grating. The program is developed indigenously and can be used on a PC. The tangent error and microroughness of the mirrors is explicitly accounted for in the program. The wavelength dependent absorption of radiation at the different reflecting surfaces is also included for calculations of the optical throughput. The dependence of the final image line shape and resolution on various beam line parameters is calculated. The results are useful in deciding the tolerances of the various beam line components and their positions.

Keywords. Synchrotron radiation; ray tracing; image characteristics.

PACS No. 42·15

1. Introduction

Indus-1 is the first synchrotron radiation source in India coming up at the Centre for Advanced Technology, Indore with a 450 MeV electron storage ring. From the bending magnets, useful flux is available in the wavelength range of 15 Å to 1600 Å and beyond, the critical wavelength being 61 Å [1]. One of the beamlines will be used for X-ray spectroscopic studies employing radiation in a wide energy range of 20 to 1200 eV. The beamline is meant for high resolution studies with a good spectral purity i.e. minimal harmonic content. Plane grating monochromator (PGM) of SX-700 type seems to be the best choice for achieving this goal [2–4].

In PGM, the plane grating is preceded by a plane mirror in such a way that the incident radiation falls on the same spot on the grating for different angles of incidence in the grazing incidence geometry. For a fixed exit slit this plane mirror is given linear and rotary motions so that the distance of the virtual source to the focussing post-mirror remains unchanged. Riemer and Torge [5] have demonstrated that these linear and rotary motions can be replaced by a rotation of the plane mirror around a suitable axis of rotation outside the plane of the mirror so that the radiation can be reflected to the same point on the grating, for three angular positions $(\alpha_1, \alpha_2, \alpha_3)$ of the plane mirror. The analytical formulation of this problem was given by Pimpale *et al* [6] which gives an exact algebraic theory of the relationship between the geometric parameters of the plane mirror-grating system and the $\alpha_1, \alpha_2, \alpha_3$ angles.

One can choose the angles based on the wavelength region of interest and reflectivity of the mirror surfaces.

A modification of SX-700 beam line has been discussed by Nyholm *et al* [7] in which an elliptical pre-mirror and an elliptical post-mirror decouple the horizontal and vertical focussing. The line image then has a minimal distortion. We have developed the optical design of a PGM using the analytical formulation of Pimpale *et al* [6] for the plane mirror-grating system and elliptical pre- and post-mirrors. Wavelength scanning is achieved by changing the glancing angle of incidence on the grating and the exit angle consistent with the focussing condition $\sin\beta/\sin\alpha \equiv C =$ constant. The detailed design is reported in [8].

In the present work, ray tracing program is developed indigenously for this beam line. Absorption of intensity at every reflection as a function of incidence angle and the refractive index $(n + ik)$ of the mirror surface is considered for every ray using Fresnel's formulae [9]. The wavelength dependence of the refractive index is explicitly taken into consideration. The tangent error in the reflecting surface is included. Absorption of intensity due to the micro-roughness of the surface is also accounted for [10]. The line shape is obtained from the spot diagram by taking its X and Y profiles. In PGM, different wavelengths are scanned by changing the angle of incidence on the plane mirror. Keeping a particular θ fixed corresponding to a wavelength one can look for the different wavelengths that are admitted at the exit slit, thereby yielding information about the wavelength mixing i.e. resolution governed by geometric factors. Such a resolution is calculated by considering intensities of different wavelengths around the central wavelength for a given slit width. Finally, the program is used for finding the tolerances in positioning of different optical elements.

Programs such as the RAY (Bessy, Berlin) and SHADOW (Wisconsin) are widely used for beam line ray tracing purposes. These programs run on main frame machines and the source code is usually not available. We, therefore, thought it worthwhile to develop indigenously ray tracing program for this work. Our program being based on analytical considerations is simple enough to be implemented on a PC. Further we have also included the features of intensity calculations as well as wavelength resolution as mentioned above. To the best of our knowledge, we are reporting here for the first time the final image shape for a complete PGM beamline comprising the pre- and post-elliptical mirrors and the SX-700 type plane mirror-grating combination with the inclusion of (i) specular reflectivity, (ii) micro-roughness scatter and (iii) wavelength broadening due to geometrical factors.

We have carried out explicit calculations by taking all the reflecting surfaces to be gold. The value of the constant C employed in these calculations is 2·25; this value gives a good grating efficiency and is commonly employed in the design of various SX 700 beam lines. All the calculations correspond to a grating with 1200 grooves per mm and for a good image 10,000 rays are traced.

A preliminary report of part of this work is given in [11].

2. The beam line simulation

The schematic diagram of the PGM beam line under consideration is shown in figure 1. EM1 and EM2 are elliptical pre- and post-mirrors, PM is the plane mirror and G is the plane grating. The extended source S is simulated by taking random points within the source size at S. A ray is simulated by joining a random point at S with another random point on EM1. For ray tracing purposes, the general pre-

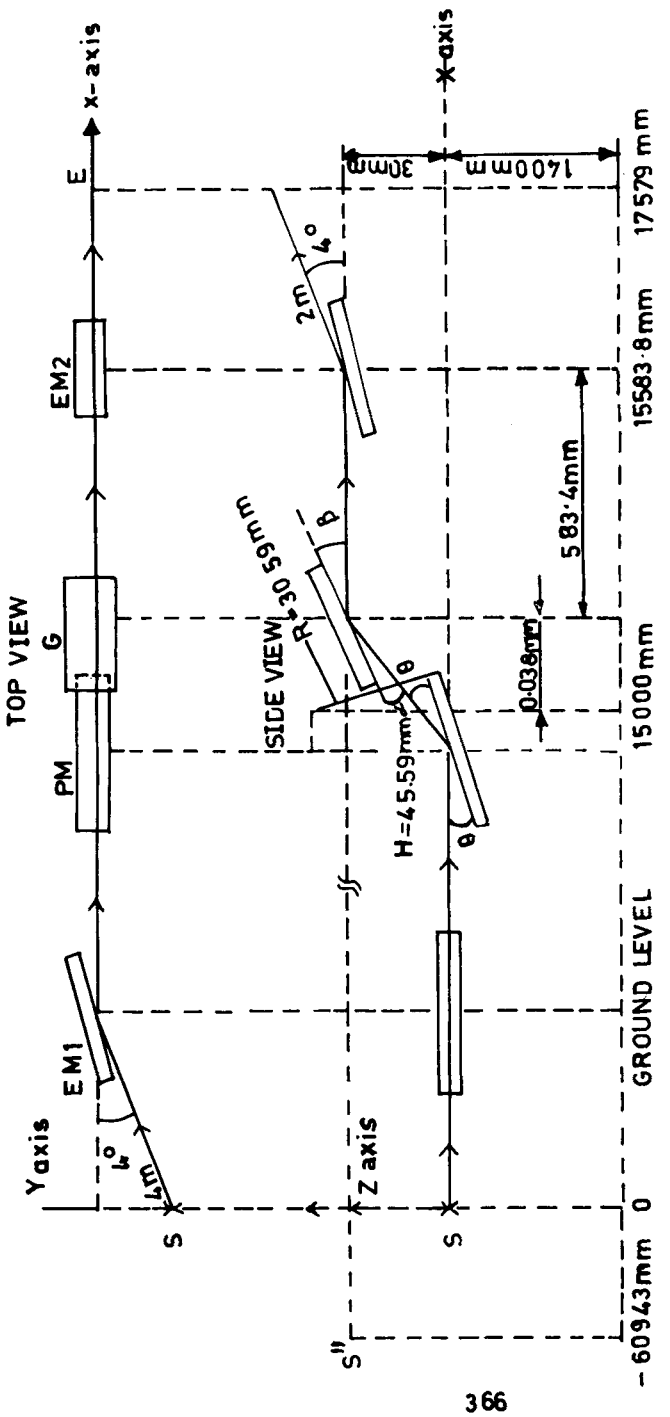

Figure 1. Schematic arrangement of complete beam line with dimensions. S is the exit slit on the storage ring, EM1 and EM2 are the pre- and post-elliptical mirrors, PM and G stand for the plane mirror and plane grating of the dispersing system.

scription of Spencer and Murty [12] is followed. Only the first order diffraction is considered. The mathematical formulation is described in Appendix.

Starting with initial intensity I (say 1) for any ray, the intensity is modified at every reflection as per Fresnel formulae. The electron storage ring orbit is in the horizontal plane and most of the incident radiation is polarized with electric field vector in the same plane. Thus for EM1 the electric vector is in the plane of incidence whereas for PM and EM2 it is orthogonal to the plane of incidence. The change of polarization due to the vertical divergence of the incident beam is ignored for simplicity. The wavelength dependent values of the refractive index $(n + ik)$ for the reflecting surface gold are from Lynch and Hunter [13].

Micro-roughness effect on the reflected intensity I' is calculated using the Johnson formula,

$$I' = I \exp(-(4\pi\sigma \cos\theta/\lambda)^2).$$

Here θ is the angle of incidence, I is the incident intensity at wavelength λ and σ is the RMS micro-roughness.

The tangent error in the surface is simulated by deviating the normal to the plane randomly through an angle within the bounds of maximum tangent error. From the spot diagram of the final image the X- and Y-profiles of the image are obtained.

For wavelength resolution at the central wavelength corresponding to angle of incidence θ on PM, we proceed as follows. Consider a wavelength step of width $\delta\lambda = 0{\cdot}001\lambda$ and calculate explicitly the image at the final image-plane for different wavelengths

$$\lambda_n = \lambda + n\delta\lambda,$$

where n takes a number of integral positive and negative values keeping the same θ. On specifying the upper and lower edges of the exit slit, the program computes intensities of each λ_n within the exit slit. A plot of this intensity as a function of wavelength gives the line shape and resolution.

Positioning of any element can be varied from its ideal value (see figure 1). The spread of the image in horizontal and vertical positions in the final image plane is obtained. From this the tolerances in positioning of the different optical elements in the beamline are found.

3. Results

The ideal positions of the optical components and other parameters used for ray tracing are collected together in table 1. The spot diagram and the vertical and horizontal line shapes for a typical wavelength $\lambda = 48{\cdot}8$ Å are shown in figure 2. The vertical line width is 53 μ and the horizontal line width is 1 mm for a source size of 0·25 mm × 0·25 mm using parameters from table 1.

The reduction in intensity in the final image as a result of (i) absorption during specular reflection and (ii) absorption due to micro-roughness is computed for different wavelengths λ in the region 12·2 Å to 110 Å. Table 2 shows the final % intensity transmitted. For all these calculations, the angle of incidence is always greater than the critical angle for total reflection. We have taken the dimensions of the optical components to be sufficiently large so that no ray is lost during reflection or diffraction. In this situation, the tangent error within the commercially available accuracy of

Table 1. PGM beam line parameters (see figure 1).

Source size	0·25 × 0·25 mm^2
Number of rays traced	10,000
Source to EM1 distance	4,000 mm
Length of EM1	114·6 mm
Breadth of EM1	1 mm
Major axis, *a*1	8,794·2 mm
Minor axis, *b*1	257·2 mm
Tan-error of EM1	1 arc sec
RMS roughness of EM1	2 nm
Glancing angle of incidence of EM1	2 deg.
Lengh of plane mirror	100 mm
Breadth of plane mirror	40 mm
Tan-error of plane mirror	1 arc sec
RMS roughness of plane mirror	1 nm
Length of grating	186 mm
Breadth of grating	40 mm
X-position of centre of rotation, L	15,000 mm
Z-position of centre of rotation, H	45·6 mm
Radius of arm of rotation, R	30·6 mm
Number of grating elements	1,200 grooves/mm
X-position of EM2	15,583·8 mm
Z-position of EM2	30 mm
Major axis of EM2, *a*2	39,263·2 mm
Minor axis of EM2, *b*2	431·5 mm
Length of EM2	350 mm
Breadth of EM2	40 mm
Tan-error of EM2	1 arc sec
RMS roughness of EM2	2 nm
X-position of image plane	17,578·6 mm

Table 2. The percentage intensity, I at the image plane for different wavelengths with and without the inclusion of roughness, σ (2 nm RMS) and the imaginary part of the dielectric constant k of the reflecting coating gold ($I = 100$ when $k = 0, \sigma = 0$).

Wave-length Å	I for $k \neq 0, \sigma = 0$	I for $k = 0, \sigma \neq 0$	I for $k \neq 0, \sigma \neq 0$
12·2	12·5	29·2	3·65
23·9	11·5	69·3	7·97
31·2	12·0	79·1	9·49
48·8	27·6	89·13	24·60
70·3	49·2	93·49	46·00
95·8	76·3	95·94	73·20
110·0	76·8	96·61	74·20

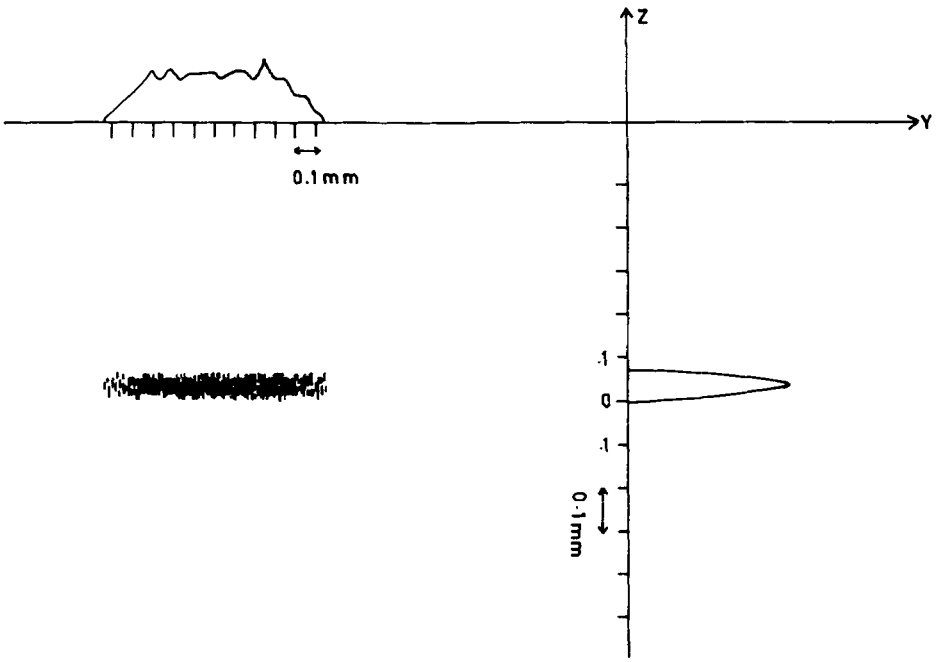

Figure 2. Spot diagram and vertical (Z) and horizontal (X) line profiles for $\lambda = 48{\cdot}8$ A for ideal positions of the optical components.

Table 3. Change in the final image position for changes in the ideal positions of various optical components for three typical photon energies.

Change δd (mm)	Change in image position (mm) 1015·7 eV	253·8 (eV)	112·7 (eV)
(a) Changing the source – EM1 distance, $d = 4000$ mm			
1	0·06	0·08	0·08
−1	−0·074	−0·07	−0·05
(b) Changing the x-position of the centre of rotation, $X = 15{,}000$ mm			
150	−0·001	−0·001	−0·001
−150	0·001	0·001	0·001
(c) Changing the Z-position of the centre of rotation, $Z = 45{\cdot}59$ mm			
−0·1	0·016	0·014	0·015
0·1	−0·015	−0·015	−0·015
(d) Changing the radius of the arm of rotation, $R = 30{\cdot}59$ mm			
−0·1	−0·013	−0·012	−0·012
0·1	0·013	0·012	0·011
(e) Changing the X-position of EM2, $X = 15{,}583{\cdot}8$ mm			
−0·5	0·034	0·034	0·034
0·5	−0·035	−0·034	−0·034
(f) Changing the Z-position of EM2, $Z = 30$ mm			
−0·01	−0·011	−0·011	−0·010
0·01	0·009	0·010	0·010

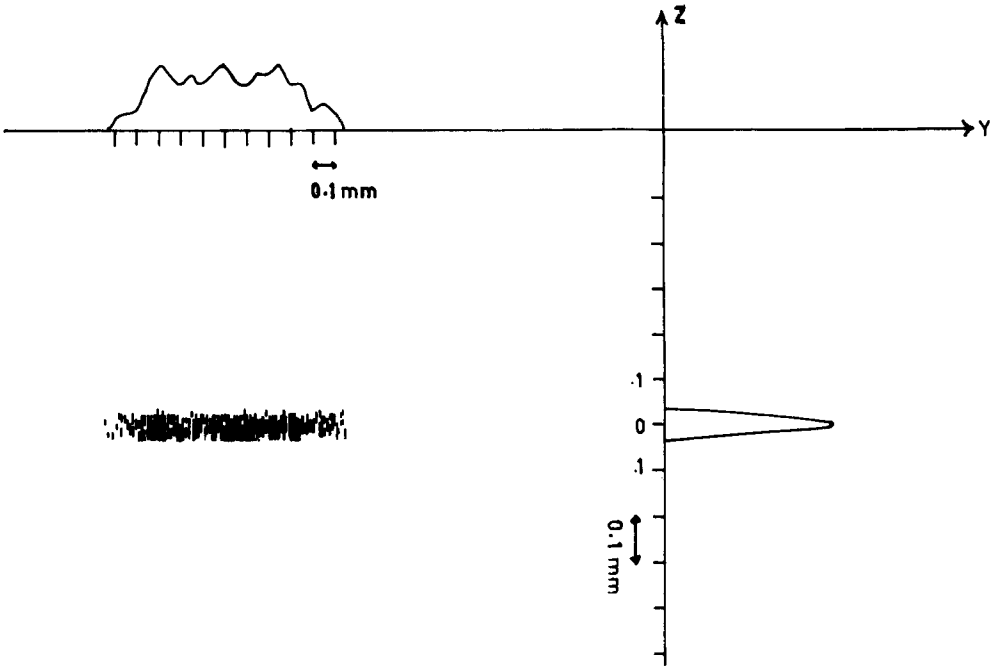

Figure 3. Spot diagram and vertical (Z) and horizontal (X) line profiles for $\lambda = 48{\cdot}8$ A when the X-position of EM2 is varied by $\delta X = -0{\cdot}5$ mm.

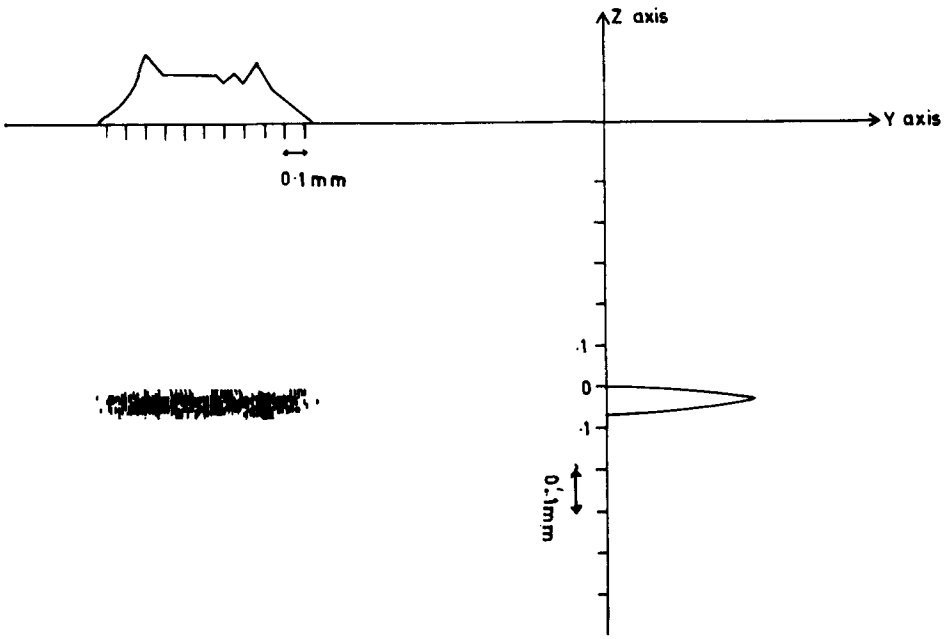

Figure 4. Spot diagram and vertical (Z) and horizontal (X) line profiles for $\lambda = 48{\cdot}8$ A when the X-position of EM2 is varied by $\delta X = 0{\cdot}5$ mm.

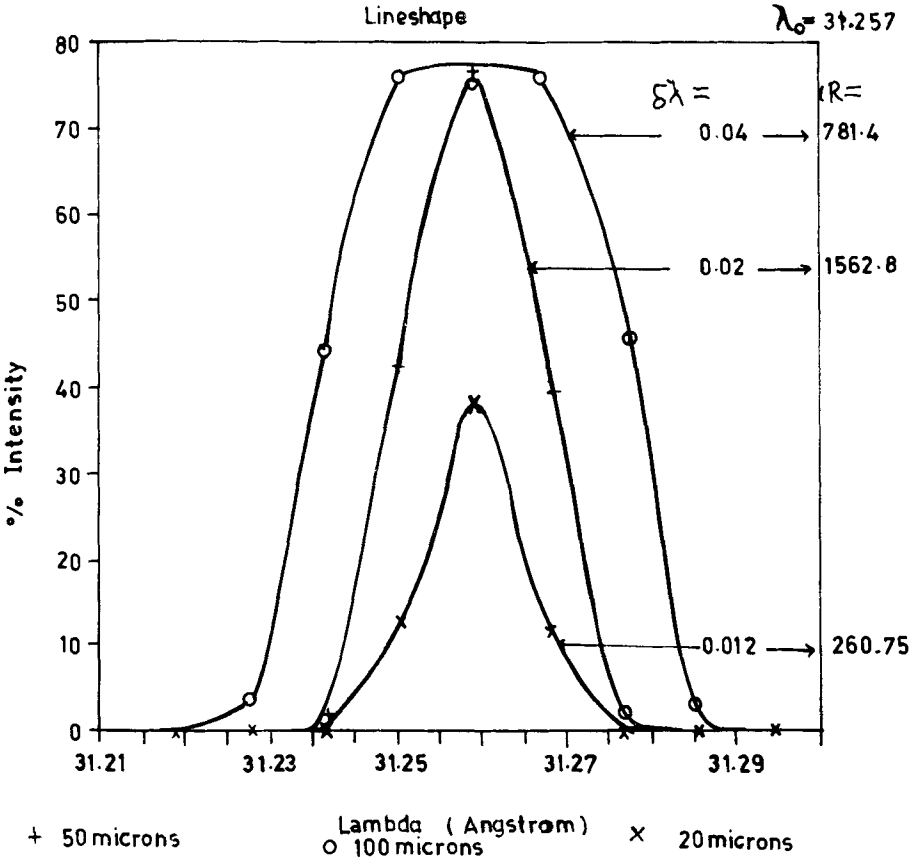

Figure 5. Lineshape for wavelength $\lambda = 31{\cdot}26$ A for three slit widths 20, 50 and 100 microns respectively.

1 arc sec does not affect the intensity. Also, the diffraction grating is assumed to have 100% reflection in the first order. Table 2 clearly shows that both the micro-roughness and absorption effects reduce intensity substantially for lower wavelengths, the latter being dominant for the assumed value of σ.

Table 3 shows the effects of variations in (i) the position of pre-mirror with respect to source S, (ii) the position of mirror-grating system along X-direction, (iii) the position of mirror-grating system along Z-direction, (iv) radius of rotation arm, (v) position of post-mirror along X-direction and (vi) position of post-mirror along Z-direction.

The variations listed are for significant changes in the mean image position and/or the image spread. To exemplify the image shift with variation in a parameter, figures 3 and 4 show the spot diagrams and the horizontal and vertical profiles of the images for typical cases: For $\lambda = 48{\cdot}85$ Å the x-position of EM2 is varied with $\delta x = -0{\cdot}5$ mm (figure 3) and $\delta x = +0{\cdot}5$ mm (figure 4). Figures 5 and 6 show the intensities of wavelengths 95·73 Å and 31·21 Å respectively for three slit-widths 20, 50 and 100 microns. The corresponding line shapes can be discerned from the figures. The resolution $RS = \lambda/\Delta\lambda$, where $\Delta\lambda$ is half the line width, is given in table 4.

Corresponding to λ the angle θ may be in error, say $\delta\theta$, which causes the shift in the image of λ in vertical direction. Figure 7 gives the vertical position (mean z) of

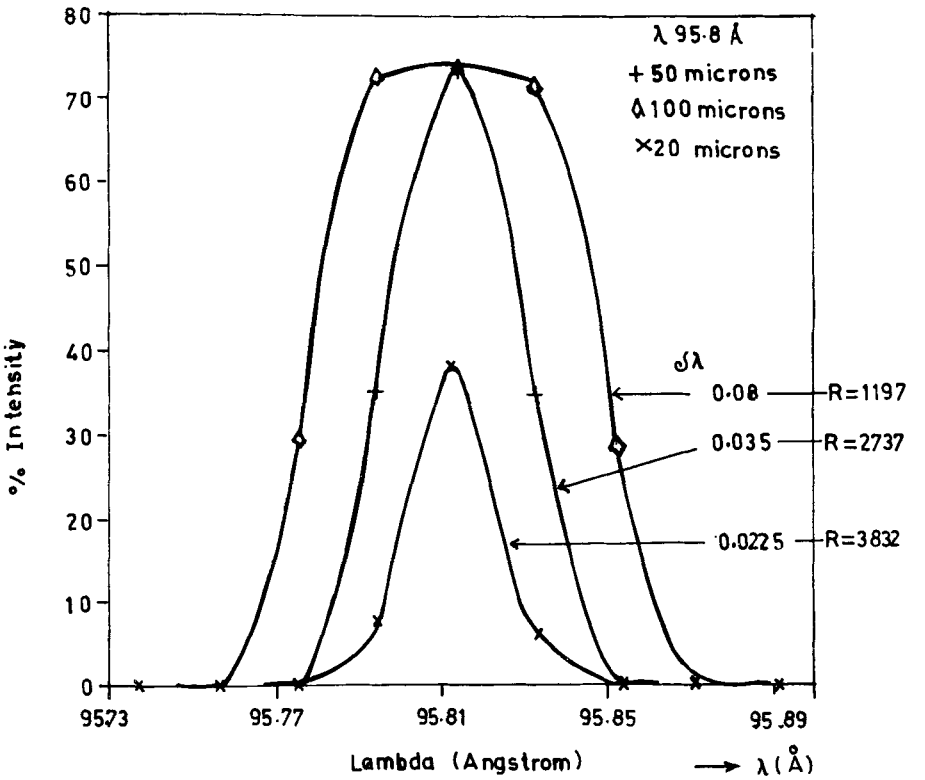

Figure 6. Lineshape for wavelength $\lambda = 95{\cdot}8$ A for three slit widths 20, 50 and 100 microns respectively.

Table 4. Resolution RS ($= \lambda/\Delta\lambda$) as calculated from figures 5 and 6 for different exit slit widths.

Wavelength Å	Slit width (microns) 20	50	100
31·257	2604·7	1562·8	781·4
95·8	3832	2737	1197

the image as a function of error $\delta\theta$ for three different wavelengths. We note that the shift is linear with respect to $\delta\theta$ and it is not very sensitive to wavelength.

The size of the image varies with the position of the image plane along the X-direction. Sample chamber may be placed beyond the exit slit to illuminate, say 1 mm × 1 mm sample uniformly. Figure 8 gives the image spread (vertical width) for different image plane positions to facilitate the positioning of the sample.

4. Discussion and concluding remarks

We note that the beam line throughout decreases substantially with increasing energy—hardly 4% of the incident intensity is available at an energy of 1016 eV when

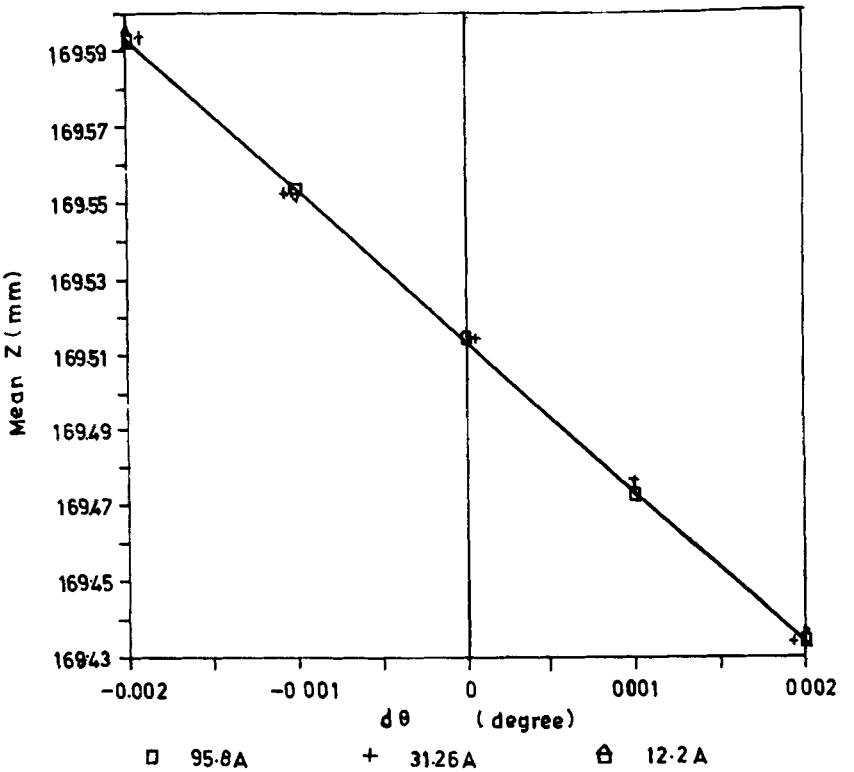

Figure 7. Position (mean Z) of the image as a function of the variation $\delta\theta$ around θ for three different wavelengths.

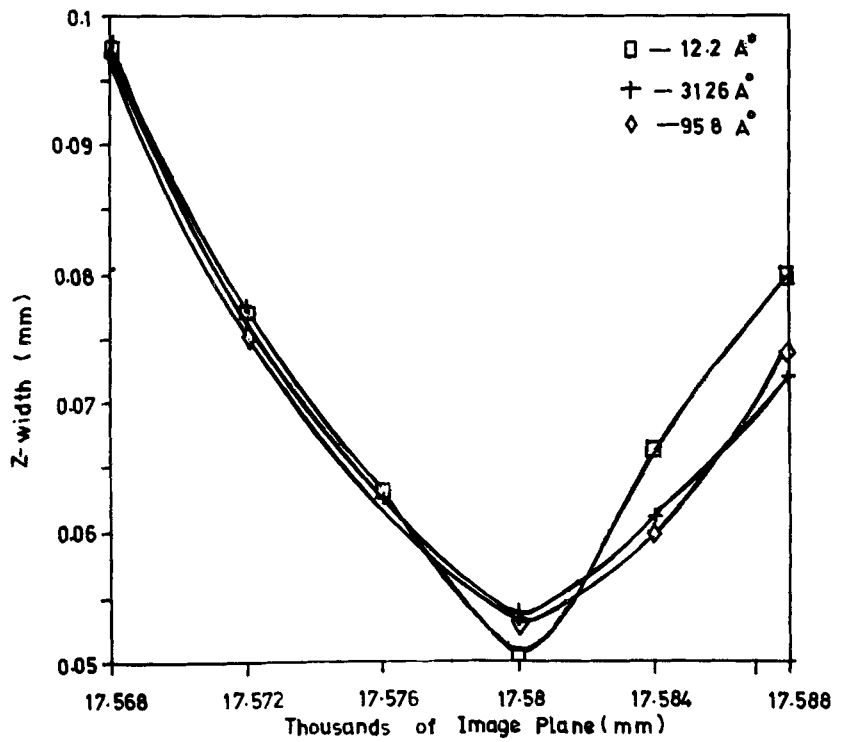

Figure 8. Vertical spread of the image for different image plane positions.

both microroughness and absorption at the reflecting surfaces is taken into account. Within the commercially available smoothness of 2 nm, the absorption effect is the more dominant of the two. Another feature of interest that comes out is the wavelength independence of the positioning accuracy of various optical components. Thus one can do alignment with an optical wavelength, say by employing a laser radiation. The final alignment for XUV radiation from the synchrotron would then require only very minor changes. From amongst the various optical components, an inaccuracy in the x-position of the PM-grating system is not very serious; e.g. a shift of 150 mm changes the image position by only 0·001 mm. On the other hand a change of 0·1 mm in the z-position of the same shifts the image by 0·01 mm.

Acknowledgement

Thanks are due to V G Bhide, R Srinivasan, V B Sapre, S M Chaudhari, S K Deshpande, R V Nandedkar, K J S Sawhney, N C Das and R Nyholm for help during the progress of this work.

Appendix

Schematics of ray tracing formulation

Ray tracing essentially involves determination of the path of light rays through an optical system comprising of various optical elements such as mirrors, lenses, apertures, gratings. This is done with the help of elementary geometry by successive application of the law of reflection (or refraction or diffraction) as the ray encounters the optical element. The incident ray is defined in a coordinate system S_0 [for extended sources we take the central point of the source as origin] as starting from a source point $\mathbf{x}_0$ moving in a direction specified by direction cosines $\mathbf{l}_0$. In our case the source is confined to YOZ plane of S_0. The point $\mathbf{x}_0$ is then generated by two random numbers within the domain specified by the source dimensions, the X-coordinate being identically zero. The central ray is prescribed by the position of the centre of the optical element; in the present case this means

$$\mathbf{l}_0(\text{central ray}) = (1, 0, 0). \tag{A1}$$

Two other random numbers are used to generate an arbitrary direction within pre-assigned horizontal and vertical divergences around the central ray. An arbitrary point $\mathbf{x}$ on the ray is then given by the parametric equations:

$$\mathbf{x} = \mathbf{x}_0 + \mathbf{l}_0 t. \tag{A2}$$

The first optical element, EM1 in the present case, is described by an equation, say,

$$f(\mathbf{x}_1) = 0 \tag{A3}$$

in a coordinate system S_1 with origin at the centre of the optical element and suitably chosen coordinate axes. We transfer the coordinate system from S_0 to S_1 using the transformation equations:

$$\mathbf{x}_1 = \mathbf{a} + T\mathbf{x}_0, \tag{A4}$$

where **a** are the coordinates of the origin of S_0 with respect to S_1 and T is the transformation matrix given by

$$T_{ij} = e_i^1 \cdot e_j^0. \tag{A5}$$

$e_i^1, e_i^0\ i = x, y, z$ are the unit vectors along the coordinate axes of S_1 and S_0. The direction cosines are transformed as

$$\mathbf{l}_1 = T\mathbf{l}_0. \tag{A6}$$

The next step is to calculate the point $\mathbf{x}_M$ at which the ray intersects the optical element. For simple systems, this is readily obtained by solving

$$f(\mathbf{x}_1 + \mathbf{l}_1 t) = 0 \tag{A7}$$

for $t = t_M$. Then

$$\mathbf{x}_M = \mathbf{x}_1 + \mathbf{l}_1 t_M. \tag{A8}$$

For simple surfaces, like aperture planes, equation (A7) can be analytically solved. However, for curved surfaces one has to employ an iterative procedure. Using the subscript j to denote the iteration number, we write

$$t_{j+1} = t_j - f(\mathbf{x}_j)/f'(\mathbf{x}_j), \tag{A9}$$

where

$$\mathbf{x}_j = \mathbf{x}_1 + \mathbf{l}_1 t_j \tag{A10}$$

and

$$f'(\mathbf{x}_j) = \mathrm{d}f/\mathrm{d}t|_{t=tj}. \tag{A11}$$

The most useful starting point for the iteration scheme is provided by the point of intersection of the incident ray and the tangent plane at the centre of the optical surface.

The next step is to describe the interaction at the optical surface. In our case we have either reflection or diffraction by a reflection grating. For both we need the unit normal $\mathbf{N}(\mathbf{x}_M)$ to the optical surface at the point of intersection $\mathbf{x}_M$. This is given by

$$\mathbf{N}(\mathbf{x}_M) = \pm \operatorname{grad} f/|\operatorname{grad} f|\Big|(\mathbf{x} = \mathbf{x}_M). \tag{A12}$$

The sign of the normal is so chosen that it points outwards from the reflecting/diffracting surface. For plane mirror and plane grating $\mathbf{N}$ is independent of $\mathbf{x}_M$. For reflection the outgoing rays have direction cosines $\mathbf{l}_r$ given by

$$\mathbf{l}_r = \mathbf{l}_1 + 2|\mathbf{l}_1 \cdot \mathbf{N}|\mathbf{N} \tag{A13}$$

and for diffraction these are given by

$$\mathbf{l}_d = \mathbf{l}_1 - \Lambda\mathbf{u} + \gamma\mathbf{N}, \tag{A14}$$

where

$$\Lambda = n\lambda/d(\mathbf{x}_M) \tag{A15}$$

$$\gamma = -\mathbf{l}_1 \cdot \mathbf{N} + [(\mathbf{l}_1 \cdot \mathbf{N})^2 - \Lambda^2 + 2\Lambda\mathbf{l}_1 \cdot \mathbf{u}]^{1/2} \tag{A16}$$

with $\mathbf{u}$ the unit normal to the rulings of the diffraction grating, $d(\mathbf{X}_M)$ the grating

spacing in the neighbourhood of $\mathbf{x}_M$, n the order of diffraction and λ the radiation wavelength. Equation (A14) simplifies for the case of plane grating since d and $\mathbf{N}$ then become constants. Thus the outcoming ray from the optical element is described parametrically by

$$\mathbf{x} = \mathbf{x}_M + \mathbf{l}_{r(d)}\mathbf{t}. \tag{A17}$$

The above procedure is repeated to trace the rays further until one encounters the final image plane. The points of intersection of the outgoing rays with the image are plotted to get the spot diagram.

References

[1] S S Ramamurthi, *Proc. Int. Conf. Synchrotron Radiation Sources*, Feb. 1992, Centre for Advanced Technology, Indore, p 9

[2] H Petersen, *Opt. Commun.* **40**, 402 (1982)

[3] H Petersen, *Soft X-ray optics and technology*, SPIE **733**, 262 (1986)

[4] M Domke, T Mandel, A Puschmann, C Xue, D A Shirley, G Kaindl, H Petersen and P Kuske, *Rev. Sci. Instrum.* **63**, 80 (1992)

[5] F Reimer and R Torge, *Nucl. Instrum. Methods.* **208** 313 (1983)

[6] A V Pimpale, S K Deshpande and V G Bhide, *Appl. Opt.* **30**, 1591 (1991)

[7] R Nyholm, S Svensson and J Nordgren, *Nucl. Instrum. Methods* **A246**, 267 (1986)

[8] A Pimpale, C Mande, B D Padalia, A S Nigavekar, V B Sapre, R Shankar and V G Bhide, *Beam line for photo-absorption studies using synchrotron radiation source INDUS 1*, Inter-University Consortium for DAE Facilities, Indore, Report (unpublished) June 1990

[9] M Born and E Wolf, *Principles of Optics (6th Ed.)* (Oxford, Pergamon Press, 1980)

[10] R L Johnson in *Handbook on synchrotron radiation* edited by E Koch (Amsterdam, North Holland, 1983), Vol. **1A** p. 180

[11] A V Pimpale, S K Deshpande, V S Edlabadkar, V B Sapre and V G Bhide, *Proc. Int. Conf. Synchrotron Radiation Sources, Feb 1991*, Centre for Advanced Technology, Indore, p. 364 (1992)

[12] G H Spencer and M V R K Murty, *J. Opt. Soc. Am.* **52**, 672 (1962)

[13] D W Lynch and W R Hunter in *Handbook of Optical Constants of Solids* edited by E D Palik (Orlando, Academic Press, 1985) p. 275